Article

Evaluation of Fenton, Photo-Fenton and Fenton-like Processes in Degradation of PE, PP, and PVC Microplastics

Kristina Bule Možar [1], Martina Miloloža [1], Viktorija Martinjak [1], Floren Radovanović-Perić [1], Arijeta Bafti [1], Magdalena Ujević Bošnjak [2], Marinko Markić [1], Tomislav Bolanča [1], Matija Cvetnić [1], Dajana Kučić Grgić [1,*] and Šime Ukić [1]

[1] Faculty of Chemical Engineering and Technology, University of Zagreb, Trg Marka Marulića 19, 10000 Zagreb, Croatia; kbule@fkit.unizg.hr (K.B.M.); miloloza@fkit.unizg.hr (M.M.); vprevaric@fkit.unizg.hr (V.M.); fradovano@fkit.unizg.hr (F.R.-P.); abafti@fkit.unizg.hr (A.B.); mmarkic@fkit.unizg.hr (M.M.); tbolanca@fkit.unizg.hr (T.B.); mcvetnic@fkit.hr (M.C.); sukic@fkit.unizg.hr (Š.U.)

[2] Croatian Institute of Public Health, Rockefellerova 7, 10000 Zagreb, Croatia

[*] Correspondence: dkucic@fkit.unizg.hr; Tel.: +385-14597238

Abstract: The global problem of microplastics in the environment is "inspiring" scientists to find environmentally friendly and economically viable methods to remove these pollutants from the environment. Advanced oxidation processes are among the most promising methods. In this work, the potential of Fenton, photo-Fenton, and Fenton-like processes for the degradation of microplastics from low-density polyethylene (LDPE), polypropylene (PP), and poly(vinyl chloride) (PVC) in water suspensions was investigated. The influence of three parameters on the efficiency of the degradation process was tested: the pH of the medium (3–7), the mass of added iron (10–50 times less than the mass of microplastics), and the mass of added H_2O_2 (5–25 times more than the mass of added iron). The effectiveness of the treatment was monitored by FTIR-ATR spectroscopy. After 60-min treatments, the PP microparticles were found to be insensitive. In the Fenton treatment of PVC and the photo-Fenton treatment of LDPE and PVC, changes in the FTIR spectra related to the degradation of the microplastics were observed. In these three cases, the treatment parameters were optimized. It was found that a low pH (3) and a high iron mass (optimal values were 1/12 and 1/10 of the mass of the microplastics for LDPE and PVC, respectively) favored all three. The degradation of LDPE by the photo-Fenton treatment was favored by high H_2O_2 concentrations (25 times higher than the mass of iron), while these concentrations were significantly lower for PVC (11 and 15 times for the Fenton and photo-Fenton treatment, respectively), suggesting that scavenging activity occurs.

Keywords: microplastics; low-density polyethylene; polypropylene; poly(vinyl chloride); advanced oxidation; Fenton-based processes

1. Introduction

The global development of human society has undoubtedly increased the quality of human life, which is mainly reflected in the prolongation of human life [1,2] and the increase in the world population [3]. On the other hand, this development has led to excessive environmental pollution [4,5], which is a threat to all living organisms, including human beings. One anthropogenic pollutant that has recently become the focus of scientific interest is plastic, especially plastic particles smaller than 5 mm, known as microplastic (MP) particles or simply microplastics (MPs) [6,7]. MPs have so far been detected in various parts of the environment, including in the air [8], soil [9], and water [10]. Because of the high bioavailability of MPs in aquatic medium [11], contamination of this environment is of particular interest to scientists. MP particles can be easily ingested by aquatic organisms and, thus, enter the food chain. Particles bellow 150 μm can be absorbed by biota tissue, organs, and even cells [12]. This leads to a bioaccumulation effect. While it is suspected that there should also be a biomagnification effect, the studies conducted to date have not

been able to confirm this [11,13,14]. The adverse potential of MPs has been demonstrated in numerous studies [12,15–17], so it is not surprising that MPs are considered an emerging contaminant [18].

In recent decades, scientists have conducted intensive research into methods that effectively remove MPs from the environment. Of the approaches tested, biological treatment is considered the most environmentally friendly. However, due to the extreme stability of plastics and the hydrophobicity of their surface, it is difficult to find organisms that degrade plastics quickly and efficiently [19]. Another approach is to use membrane processes. However, it has been shown that the removal of MPs using membrane technology is still incomplete [20], and there is also a problem with membrane maintenance and sludge disposal. Recently, the applicability of advanced oxidation processes (AOPs) has been increasingly investigated as an additional option for treating water contaminated with MPs. The basis of AOP treatments is the formation of extremely reactive radicals (strong oxidizing agents), which ensure rapid reaction rates in the degradation of recalcitrant organic pollutants. This approach has a low selectivity and can, therefore, be used for the simultaneous degradation of different pollutants [21]. AOP treatment can lead to partial degradation or, ideally, complete mineralization of the pollutants. Partial degradation usually results in the formation of less complex chemical forms that are more susceptible to other treatment approaches, especially biodegradation, which is the most environmentally friendly approach. For this reason, AOPs are often used in combination with biodegradation as a pretreatment step [22,23].

The AOP studies available in the literature generally do not report complete mineralization of the MPs and focus the discussion on the degree of polymer degradation achieved. Ortiz et al. [24] investigated the effect of Fenton treatment on various MPs samples (polyethylene (PE), polypropylene (PP), poly(vinyl chloride) (PVC), polyethylene terephthalate (PET), and expanded polystyrene (EPS)) in a size range of 150–250 μm obtained from commercially available plastic products. The initial mass of the MPs was 100 mg, the iron concentration was 10 mg/L, and the H_2O_2 concentration was 1000 mg/L. The treatment lasted 7.5 h. During the treatment, additional amounts of iron and H_2O_2 were added to the system at regular intervals to recover the consumed reagents. After the treatment under environmental conditions (pH and temperature) showed no changes in the samples, they decided to perform the treatment under more extreme conditions: an acidic medium with a pH of 3 and elevated temperature (80 °C). This treatment resulted in a mass loss of about 8 to 12%. Lang et al. [25] investigated the effect of Fenton treatment (7 days, room temperature, pH 4) on the adsorption of heavy metals on the surface of PS MPs and reported that the applied treatment contributes to the aging of MPs. Piazza et al. [26] studied the environmental aspects of a photo-Fenton treatment of PP and PVC MPs (the samples had a size of 155 and 73 μm, respectively). The treatment involved visible light irradiation and the application of ZnO nanorods coated with a SnO_x layer and decorated with Fe^0 nanoparticles. The authors monitored the changes in the FTIR spectra to determine the percentage of degradation of the MPs. After 7 days of treatment, a degradation efficiency of 94–96% was observed. Miao et al. [27] reported a 56% mass loss of PVC microparticles with a size of 100–200 μm and a 75% dechlorination after 6 h treatment with an electro-Fenton-like system based on a TiO_2/graphite cathode. They also observed a significant positive contribution of temperature increase to the degree of dechlorination. In addition, the literature also reports on the investigation of the applicability of numerous other AOP treatments [28–35].

In this study, the potentials of three Fenton-based AOPs, namely Fenton, photo-Fenton, and Fenton-like processes were evaluated for the degradation of MP particles of low-density PE (LDPE), PP, and PVC. The influence of the pH of the medium, the quantity of added oxidizing agents, and the MPs concentration on the degradation process was investigated, and the optimum treatment conditions were determined.

2. Fenton-Based Processes

AOPs based on the Fenton reaction are widely used for the oxidation of organic macro- and micropollutants [36]. Some of the main advantages of Fenton-based processes are the relatively simple process equipment, relatively inexpensive and environmentally friendly reagents, and a relatively simple treatment procedure. In addition, these processes are conducted at room temperature and atmospheric pressure, which provides an additional economic advantage. Fenton-based processes are known to be highly resistant to matrix interferences and typically result in high mineralization rates for recalcitrant organic pollutants [37–39].

The basis of Fenton-based processes is the generation of the highly reactive hydroxyl radical (•OH) with a standard redox potential of $E^0(\bullet OH/H_2O) = 2.730$ V [40]. The oxidation activity of the hydroxyl radical is related to the pH of the solution (Equation (1)), so that the redox potential of the system increases with decreasing pH.

$$\bullet OH + H^+ + e^- \rightarrow H_2O \tag{1}$$

In the classical Fenton process (Figure 1, case A), the Fenton reagent is responsible for the formation of hydroxyl radicals. The Fenton reagent is a mixture of aqueous solutions of an iron(II) salt and H_2O_2, in which hydroxyl radicals are formed according to Equation (2) [41].

$$Fe^{2+} + H_2O_2 + H^+ \rightarrow Fe^{3+} + \bullet OH + H_2O \tag{2}$$
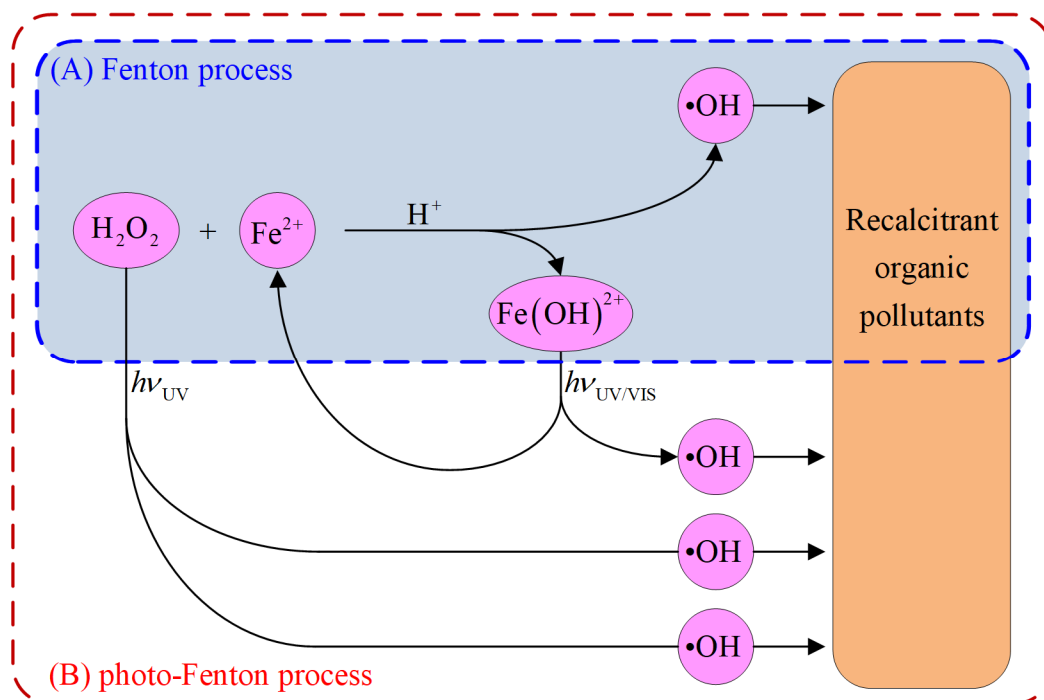
Figure 1. Schematic representation of (**A**) the Fenton process (outlined in blue) and (**B**) the photo-Fenton process (outlined in red).

The formation of hydroxyl radicals can be negatively affected by an excess of H_2O_2 or Fe^{2+} ions in the bulk (Equations (3) and (4)) [37,39], causing an undesirable scavenging effects, like the one described by Equation (5) [42].

$$\bullet OH + H_2O_2 \rightarrow HO_2\bullet + H_2O \tag{3}$$

$$\bullet OH + Fe^{2+} + H^+ \rightarrow Fe^{3+} + H_2O \tag{4}$$

$$HO_2\bullet + \bullet OH \rightarrow H_2O_2 + O_2 \tag{5}$$
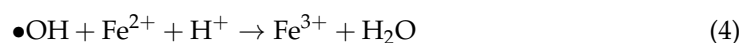
An alkaline medium is not suitable for carrying out the Fenton process because it reduces not only the oxidizing power of the hydroxyl radical but also the activity of the Fenton reagent. More specifically, at a high pH, the concentration of Fe^{2+} ions in the solution is negatively affected by the formation of iron(II) hydroxide precipitate. In addition, high pH values favor the decomposition of H_2O_2. However, very low pH values are also not beneficial for the activity of the Fenton reagent. This is because at very low pH values, the active H_2O_2 concentration is affected by the formation of stable $H_3O_2^+$ ions [43]. Therefore, in order to avoid or minimize undesirable scavenging effects and to increase the efficiency of the treatment, the process conditions must be optimized. Due to the specificity of the system to be treated, optimization should be performed for each system.

The inclusion of ultraviolet or visible light irradiation in the classical Fenton process leads to a photo-Fenton process (Figure 1, case B) in which hydroxyl radicals are increasingly produced due to a two-step reaction. First, the iron(III) ions from Equation (2) are hydrolyzed, leading to the formation of the $Fe(OH)^{2+}$ complex (Equation (6)), which subsequently undergoes photo-induced reduction and generates hydroxyl radical (Equation (7)) [44,45].

$$Fe^{3+} + H_2O \rightarrow Fe(OH)^{2+} + H^+ \tag{6}$$

$$Fe(OH)^{2+} + h\nu \rightarrow Fe^{2+} + \bullet OH \tag{7}$$

In addition, UV irradiation can cause photolysis of H_2O_2, which also increases the production of hydroxyl radicals (Equation (8)) [43].

$$H_2O_2 + h\nu \rightarrow 2(\bullet OH) \tag{8}$$

Despite the advantage of the increased production of hydroxyl radicals and the corresponding expected higher efficiency in the degradation of organic pollutants, the photo-Fenton process has some disadvantages. First and foremost, it requires irradiation during treatment, which results in high energy consumption. In addition, high concentrations of organic pollutants in a treated system can significantly reduce the absorption of irradiation by the $Fe(OH)^{2+}$ complex, resulting in an increase in irradiation time. All this makes photo-Fenton treatment much more expensive than classical Fenton treatment.

In addition to the photo-Fenton process, there are numerous other modifications of the classical Fenton process, commonly referred to as Fenton-like processes. Fenton-like processes are divided into heterogeneous and homogeneous processes. In heterogeneous Fenton-like processes, the Fe^{2+} ion in the Fenton reagent is replaced by a solid catalyst, while homogeneous Fenton-like processes refer to processes in which a different metal ion is used in place of the iron ion in combination with H_2O_2 [46]. Among heterogeneous Fenton-like systems, systems triggered by zero-valent iron, especially in the form of nanoparticles, are very popular, mainly because of their large specific surface area and high reactivity [43,47]. The process starts with the reaction between zero-valent iron and H_2O_2, leading to the formation of Fe^{2+} ions (Equation (9)), which are crucial for the formation of the hydroxyl radical (Equation (2)).

$$Fe^0 + H_2O_2 + 2H^+ \rightarrow Fe^{2+} + 2H_2O \tag{9}$$

The Fe^{3+} ions formed in the reaction described by Equation (2) additionally contribute to the formation of the Fe^{2+} ions (Equation (10)) [43].

$$Fe^0 + 2Fe^{3+} \rightarrow 3Fe^{2+} \tag{10}$$

It should be noted, however, that there is concern in the scientific community about the potential adverse effects that the presence of nanoparticles of zero-valent iron may cause in the environment [48,49].

3. Materials and Methods

3.1. Reagents and Solutions

The plastic material was purchased in the form of granules as OKITEN® 245 A (Dioki d.d., Zagreb, Croatia), GF10 (Xiamen Keyuan Plastic Co., Ltd., Xiamen, China), and GS-28 (Drvoplast d.d., Buzet, Croatia) for LDPE, PP, and PVC, respectively. Ferrous sulfate heptahydrate ($FeSO_4 \cdot 7H_2O$; ≥99%; Sigma-Aldrich, Burlington, MA, USA), elemental iron (≥95%; Carlo Erba Reagents, Milan, Italy), 30% H_2O_2 solution (1.11 g cm^{-3}; Gram-Mol d.o.o., Zagreb, Croatia), 0.1 M NaOH solution (Lach-Ner s.r.o., Naratovice, Czech Republic), and H_2SO_4 solution (Kemika, Zagreb, Croatia) at concentrations of 0.1 and 5 M were used for the AOP treatments. Ultrapure water (18.2 MΩ cm; Milli-Q, Millipore, Burlington, MA, USA) was used for all experiments.

3.2. Preparation and Characterisation of Microplastics

The purchased plastic granules were crushed in a cryo-mill (Retsch, Haan, Germany) with liquid nitrogen at an operating temperature of −196 °C. After grinding, the MPs were dried at room temperature (25.0 ± 0.2 °C) for 48 h before sieving. The ground plastic was sieved on stainless steel sieves (AS 200 jet, Retsch, Hann, Germany) to obtain MPs in the size range of 25–100 μm, which were then used for the experiments.

FTIR-ATR analysis (FTIR-8400S, Shimadzu, Kyoto, Japan, and MIRacle™ Single Reflection ATR, PIKE Technologies, Madison, WI, USA) was used to characterize the untreated MP particles and the MP particles after AOP treatments.

To gain additional insight into the MPs' degradation, the untreated MP particles and the MP particles treated under optimal conditions were analyzed by scanning electron microscopy (SEM) using a Tescan Vega Easyprobe 3 microscope (Brno, Czech Republic). Imaging was performed in secondary electron mode (SE) and backscattered electron mode (BSE) at an accelerating voltage of 10 kV and a working distance of about 8 mm. Prior to imaging, Pd/Au was sputtered onto the samples using a Quorum Technologies SC7620 sputter coater (Lewes, UK) at 18 mA for 60 s.

3.3. AOP Treatments

The experimental design for the AOP treatments (Table 1) followed the full factorial methodology with three variables tested at three levels, resulting in a total of 27 trials for each AOP treatment applied. The variables tested were pH, mass ratio of MPs to Fe, and mass ratio of H_2O_2 to Fe. Although it would be appropriate to express the amounts of iron and peroxide in the reaction system as a molar concentration (due to the fact that the potential of the system depends on the molar concentration of the substance), the AOP experiments were performed in such a way that we could only estimate the molar concentrations of these substances. Although it is known that the volume of the reaction mixture does not deviate too much from 80 mL, i.e., from the amount of added water, we cannot know the true volume of the reaction mixture because we also add a certain quantity of MPs, Fe, and H_2O_2 to the system and adjust the pH of the reaction mixtures at the beginning of the experiment. Therefore, we decided to express the amounts of the mentioned substances in the reaction system in terms of their mass instead of their molar concentration. The range of tested values (i.e., levels) was selected based on the information available in the literature [50,51]. The required masses of iron species and H_2O_2 volumes were calculated based on the mass of MPs, which was 55 mg for all experiments.

The experimental procedure was similar for all three AOP treatments. The predefined mass of 55 mg of an MPs sample was added to the reactor together with 80 mL of water. The pH was adjusted to the desired value with 0.1 M H_2SO_4, 5 M H_2SO_4, or 0.1 M NaOH, after which a certain amount of iron in a suitable form was also added to the reactor. In the Fenton and photo-Fenton treatments, ferrous ion (Fe^{2+}) was used, which was added in the form of $FeSO_4 \cdot 7H_2O$. For the Fenton-like process, elemental iron (Fe^0) was used. In the final step, an appropriate amount of 30% H_2O_2 was added to initiate the treatment. In the photo-Fenton treatment only, the reaction mixture was exposed to UV-C irradiation of 254 nm

(mercury lamp Pen-Ray® 11SC-1, UVP, Upland, CA, USA). All AOP experiments lasted 60 min, with continuous mixing at 150 rpm using a magnetic stirrer (high speed magnetic stirrer MS-3000, Biosan SIA, Riga, Latvia). After each experiment, the MPs were separated from the aqueous phase by vacuum membrane filtration through a sterile 0.45 μm cellulose nitrate membrane filter (ReliaDisc™ membrane filter, Ahlstrom, Helsinki, Finland). The MPs were then washed with water and air-dried for 24 h prior to FTIR-ATR analysis.

Table 1. Experimental design for Fenton, photo-Fenton, and Fenton-like processes.

No.	pH	m(MPs):m(Fe)	m(H_2O_2):m(Fe)	No.	pH	m(MPs):m(Fe)	m(H_2O_2):m(Fe)	No.	pH	m(MPs):m(Fe)	m(H_2O_2):m(Fe)
1	3.0	10:1	5:1	10	4.5	10:1	5:1	19	6.0	10:1	5:1
2	3.0	10:1	15:1	11	4.5	10:1	15:1	20	6.0	10:1	15:1
3	3.0	10:1	25:1	12	4.5	10:1	25:1	21	6.0	10:1	25:1
4	3.0	25:1	5:1	13	4.5	25:1	5:1	22	6.0	25:1	5:1
5	3.0	25:1	15:1	14	4.5	25:1	15:1	23	6.0	25:1	15:1
6	3.0	25:1	25:1	15	4.5	25:1	25:1	24	6.0	25:1	25:1
7	3.0	50:1	5:1	16	4.5	50:1	5:1	25	6.0	50:1	5:1
8	3.0	50:1	15:1	17	4.5	50:1	15:1	26	6.0	50:1	15:1
9	3.0	50:1	25:1	18	4.5	50:1	25:1	27	6.0	50:1	25:1

3.4. Determination of Optimal Conditions

The optimal conditions for the degradation of LDPE, PP, and PVC MPs by the three applied Fenton-based AOPs were determined using the response surface modeling (RSM) approach. The RSM approach involves a series of mathematical techniques aimed at building an empirical model that describes the relationship between the input variables (i.e., the independent variables) and one or more dependent variables (i.e., the response) [52]. Based on our experience in the field of optimization of pollutant degradation in the aquatic environment [53,54], we have assumed that a quadratic model represented by Equation (11) should be sufficient to describe the system with three independent variables and one dependent variable.

$$y = a_0 + a_1x_1 + a_2x_2 + a_3x_3 + a_4x_1x_2 + a_5x_1x_3 + a_6x_2x_3 + a_7x_1^2 + a_8x_2^2 + a_9x_3^2 \quad (11)$$

The model coefficients are denoted by a, while x_1 to x_3 represent the values of the three process parameters tested: pH, mass ratio of MPs to iron, and mass ratio of H_2O_2 to iron. In addition to the linear (x_1, x_2, x_3) and quadratic (x_1^2, x_2^2, x_3^2) contributions, the model also includes the interaction terms (x_1x_2, x_1x_3, x_2x_3) to cover the possible combined effects of the parameters tested, which, as we knew from experience [53–57], are not uncommon in such systems. The area of a broad FTIR band that occurred in the spectral range 3000–3600 cm^{-1} was used as the response, i.e., as the dependent variable y.

Statistical analysis of developed model was performed using Design-Expert 10.0 software (StatEase, Minneapolis, MN, USA).

4. Results and Discussion

First, the untreated MP samples were characterized by FTIR-ATR spectroscopy. The recorded spectra (Figure 2) clearly show the absorption bands characteristic of the polymers LDPE, PP, and PVC. The spectrum of untreated PVC (Figure 2C) contains an unexpected peak in the spectral range of 1715–1750 cm^{-1}, which corresponds to the stretching of the carbonyl group [58]. This peak obviously represents an additive present in the PVC sample tested, as pure PVC has no carbonyl groups in its structure.

Each treated sample was also analyzed by FTIR-ATR to detect changes in the intensity of the bands related to the vibrations of the groups formed during the degradation of the MPs. The formation of carbonyl species is one of the most important indicators of the oxidative degradation of MPs, and the quantification of the formed carbonyl groups by infrared spectroscopy has been the method of choice for many years due to the strong

absorption in the spectral range of 1715–1750 cm^{-1}, which is related to the stretching of the carbonyl group [58–61]. However, since the untreated PVC samples showed a peak in this region (Figure 2C), we decided not to use this band as an indicator of MPs' degradation, but rather a broad band that appeared in the spectral range 3000–3600 cm^{-1}, with a maximum at about 3370 cm^{-1}. The appearance of the band in this region indicates side reactions, such as the substitution of chloride by hydroxide [33,62] and the formation of the terminal C≡C–H group [33]. According to Liu [58], the band of OH stretching is expected in the range of 3200–3600 cm^{-1}, but the width and position of the band strongly depend on the amount of hydrogen bonding [63]. We have found several reports on the occurrence of this band during the degradation of plastics [33,62,64,65]. The stretching of the terminal C≡C–H group is expected in the range of 3250–3350 cm^{-1} [58] and may, therefore, be hidden in a broad band of OH stretching.
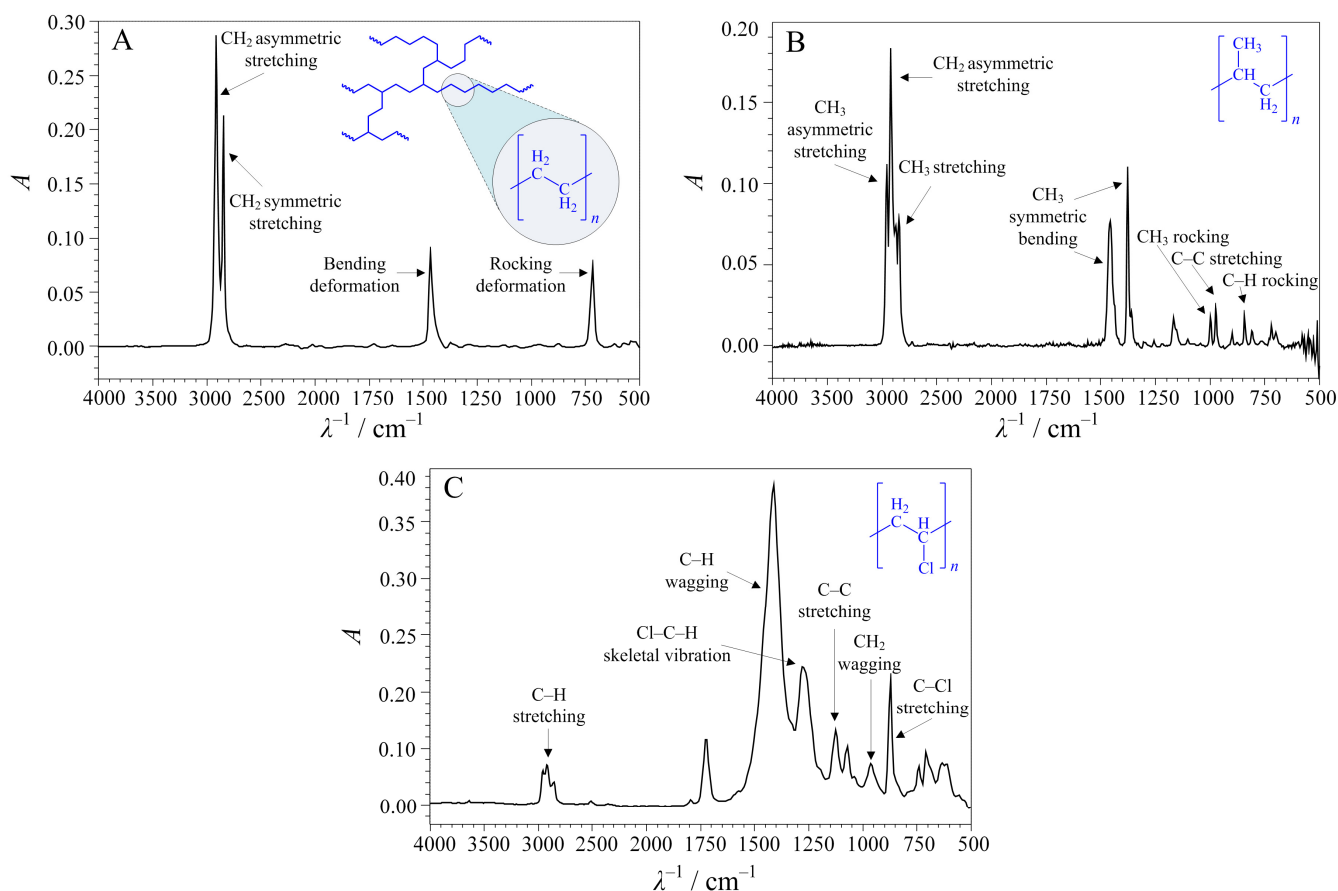
Figure 2. FTIR spectra of untreated MPs with characteristic peaks of (**A**) LDPE, (**B**) PP, and (**C**) PVC. The molecular structures of the polymers are shown in blue in the top righthand corner of each spectrum.

After analyzing the obtained FTIR spectra, it was found that some of the applied treatments, especially the Fenton-like treatment, did not result in significant spectral changes that can be associated with the degradation of MPs (Table 2). This is not so surprising, since the MPs studied are composed of polymers that do not have hydrolysable groups in their structure and are, therefore, less susceptible to degradation [66]. PP samples remained unaffected by all three treatments applied. For LDPE, only the photo-Fenton treatment led to observable changes in the intensity of the monitored band, which is apparently due to the introduction of UV-C irradiation in the treatment. Apart from the fact that the introduction of UV-C irradiation increases the production of radicals compared to the conventional Fenton process, UV-C irradiation alone may also have a significant impact

on the degradation of MPs [67]. Of the three MPs tested, PVC was found to be the most susceptible to Fenton-based treatments, with changes in the intensity of the monitored band observed for the Fenton and photo-Fenton treatments. The reason for this is most likely the chlorine atom contained in the PVC structure, which facilitates the oxidation and decomposition of PVC [66]. According to the available information, the first step of PVC decomposition should be dechlorination or dehydrochlorination, during which various chlorinated compounds can be formed [27,68]. Furthermore, dehydrochlorination leads to the formation of labile internal allyl chloride structures [69], which dissociate into chlorine radicals, Cl•, and polyene radicals, R• (Equation (12)).

$$R - Cl \rightarrow R\bullet + Cl\bullet \tag{12}$$

Polyene radicals react with oxygen from the environment and form peroxy radicals (ROO•), which can react with –CH_2– or –CH–Cl groups and, thus, contribute to the further degradation of PVC [68].

Table 2. Comparison of the experiments performed with regard to the changes observed in the FTIR bands.

Polymer	Treatment		
	Fenton	**Photo-Fenton**	**Fenton-like**
LDPE	NO	YES	NO
PP	NO	NO	NO
PVC	YES	YES	NO

Considering what is discussed above, we report here only the RSM models developed for the treatment cases that resulted in observable changes in the intensity of the monitored band. Statistical analysis of these models (Tables 3–5) confirmed their significance for describing the influence of the three variables tested. The adequacy of the models is further confirmed by the fact that 87.06 to 93.40% of the variance in the response (i.e., the independent variable), according to the R^2 values, can be explained by the variability of the values of the tested (i.e., dependent) variables. The negative values of the coefficient a_1 for all three models clearly indicate a positive influence of a more acidic environment on the efficiency of the applied treatments. The negative values of coefficient a_2 obtained for the treatments of PVC samples indicate the positive influence of a higher concentration of Fe^{2+} ions in the system, while the negative values of coefficient a_3 indicate an unfavorable influence of increased H_2O_2 concentrations, suggesting the potential scavenging effect of H_2O_2 during PVC treatment. No such effects were observed in the case of LDPE treatment.

Figures 3–5 contain graphical representations of the response surfaces corresponding to the models whose parameters are listed in Tables 3–5, while the optimal conditions for each treatment, estimated from the maxima of the response surfaces, are listed in Table 6. Visualizing the response surface of a system that has four dimensions (three independent and one dependent variable) is a challenge. Therefore, for the sake of simplicity, we decided to visualize the response surfaces at fixed values of one of the independent variables, namely pH. In this way, we enabled a transparent analysis of the behavior of the response by plotting three surfaces. In the first place, the surface trends can be seen based on the variation in the parameters m(MPs):m(Fe) and m(H_2O_2):m(Fe). Secondly, by comparing three response surfaces, it is possible to see what happens to the response due to the variation in pH. The area, A, of a broad FTIR band in the spectral range 3000–3600 cm^{-1} represents the response. The red areas on the surfaces show the most favorable conditions for performing a Fenton or photo-Fenton treatment, while the blue areas represent the least favorable conditions. The response surfaces confirm some of our conclusions derived from the statistical analysis of the RSM models. For example, the most intense red areas are obtained at a pH of 3. Furthermore, the response surfaces show that a high amount of added iron (small ratio m(MPs):m(Fe^{2+})) is beneficial not only for PVC treatment but also for

LDPE treatment. This is in line with some other reports claiming that a high concentration of Fe^{2+} ions is required for the degradation of organic pollutants by the homogeneous Fenton process [26,70]. Finally, in the case of LDPE treated with the photo-Fenton process (Figure 3), a positive effect of increased H_2O_2 concentrations is observed, with the optimal amount of added H_2O_2 being 25 times higher than the amount of added Fe (Table 6). In the case of PVC treatment, the red areas cover low to medium H_2O_2 concentrations, regardless of whether we analyze the Fenton or the photo-Fenton response surface. The optimal amounts of added H_2O_2 are estimated to be 11 and 15 times the amount of added Fe for the Fenton and photo-Fenton treatments, respectively.

Table 3. Statistical analysis of the fitted response surface model (Equation (11)) for the case of LDPE MPs treated with the photo-Fenton process. The analysis was performed with a significance of $p < 0.050$.

Model				Coefficients		Influential Variables [1]		
R^2	R^2_{adj}	F	p	Value	p	x_1	x_2	x_3
				$a_0 = 4.51$	-			
				$a_1 = -2.63$	<0.0001	YES		
				$a_2 = 0.55$	0.1534			
				$a_3 = 1.14$	0.0061			YES
				$a_4 = 2.52$	<0.0001	YES	YES	
0.8706	0.8021	12.71	<0.0001	$a_5 = -0.30$	0.5109			
				$a_6 = 0.13$	0.7692			
				$a_7 = 2.51$	0.0010	YES		
				$a_8 = -1.02$	0.1247			
				$a_9 = -0.28$	0.6640			

Note: [1] x_1 = pH; x_2 = m(MPs):m(Fe); x_3 = $m(H_2O_2)$:m(Fe).

Table 4. Statistical analysis of the fitted response surface model (Equation (11)) for the case of PVC MPs treated with the Fenton process. The analysis was performed with a significance of $p < 0.050$.

Model				Coefficients		Influential Variables [1]		
R^2	R^2_{adj}	F	p	Value	p	x_1	x_2	x_3
				$a_0 = 18.42$	-			
				$a_1 = -4.64$	<0.0001	YES		
				$a_2 = -7.12$	<0.0001		YES	
				$a_3 = -1.76$	0.0289			YES
				$a_4 = 0.44$	0.6347			
0.8994	0.8462	16.89	<0.0001	$a_5 = 0.64$	0.4879			
				$a_6 = 0.86$	0.3531			
				$a_7 = -1.70$	0.2009			
				$a_8 = 0.35$	0.7878			
				$a_9 = -3.90$	0.0071			YES

Note: [1] x_1 = pH; x_2 = m(MPs):m(Fe); x_3 = $m(H_2O_2)$:m(Fe).

Table 5. Statistical analysis of the fitted response surface model (Equation (11)) for the case of PVC MPs treated with the photo-Fenton process. The analysis was performed with a significance of $p < 0.050$.

Model				Coefficients		Influential Variables [1]		
R^2	R^2_{adj}	F	p	Value	p	x_1	x_2	x_3
				$a_0 = 22.29$	-			
				$a_1 = -5.35$	<0.0001	YES		
				$a_2 = -7.00$	<0.0001		YES	
				$a_3 = -0.76$	0.2249			
				$a_4 = -0.92$	0.2265			
0.9340	0.8990	26.72	<0.0001	$a_5 = -0.43$	0.5969			
				$a_6 = 1.06$	0.1690			
				$a_7 = -1.80$	0.1022			
				$a_8 = -0.11$	0.9185			
				$a_9 = -4.25$	0.0008			YES

Note: [1] x_1 = pH; x_2 = m(MPs):m(Fe); x_3 = m(H$_2$O$_2$):m(Fe).
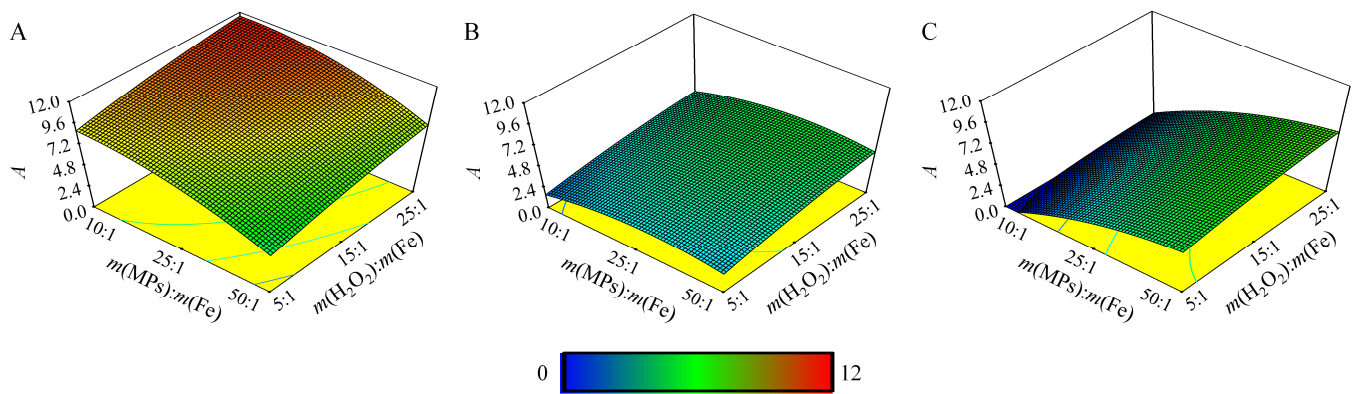
Figure 3. Obtained response surfaces for treatment of LDPE MPs by Fenton process for (**A**) pH = 3.0, (**B**) pH = 4.5, and (**C**) pH = 6.0.
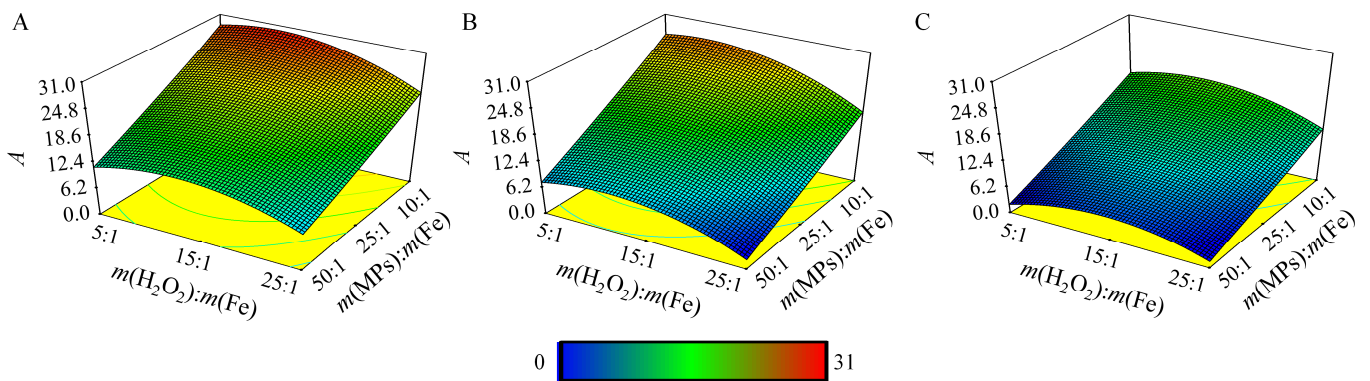
Figure 4. Obtained response surfaces for treatment of PVC MPs by Fenton process for (**A**) pH = 3.0, (**B**) pH = 4.5, and (**C**) pH = 6.0.
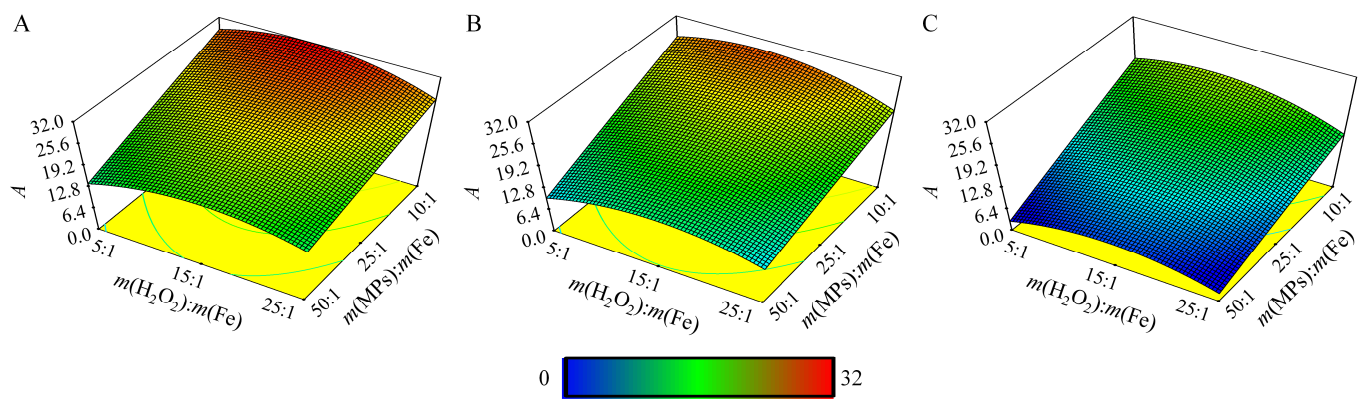
Figure 5. Obtained response surfaces for treatment of PVC MPs by photo-Fenton process for (**A**) pH = 3.0, (**B**) pH = 4.5, and (**C**) pH = 6.0.

Table 6. Optimal conditions for the treatment of MPs samples.

Polymer	Treatment	pH	m(MPs):m(Fe)	m(H_2O_2):m(Fe)
LDPE	Photo-Fenton	3	12:1	25:1
PVC	Fenton	3	10:1	11:1
	Photo-Fenton	3	10:1	15:1

For final confirmation of the results obtained, all three treatments of MPs (LDPE with Fenton and PVC with Fenton and photo-Fenton treatments) were performed under optimal conditions. The FTIR spectra and SEM images of the MPs samples after the treatments were recorded and compared with those of the untreated samples (Figures 6–8).
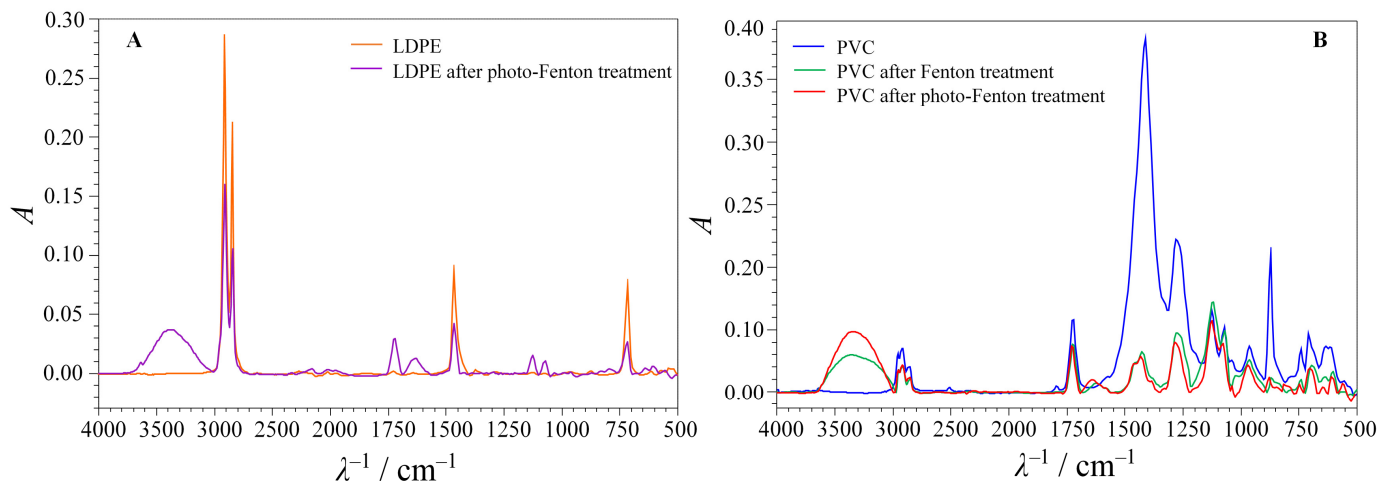
Figure 6. Comparison of FTIR spectra obtained before and after treatment under optimal conditions. The cases show (**A**) LDPE MPs and (**B**) PVC MPs.

When analyzing the FTIR spectra obtained, in addition to a clear increase in the intensity of the band in the spectral range of 3000–3600 cm^{-1} as a result of the treatments, a decrease in the intensity of the characteristic bands of LDPE and PVC polymers can also be seen. Also, a new peak appeared at 1620 cm^{-1} for all three treated samples. The peak in this region is mainly related to C=C stretching, which also indicates polymer degradation [27,71]. In the case of LDPE, the appearance of C=C structures indicates dehydrogenation as one of the degradation reactions; we found that dehydrogenation during PE degradation has also been confirmed in some other treatments [72,73]. The formation of carbonyl groups was confirmed by a new peak at 1715 cm^{-1} (Figure 6A).
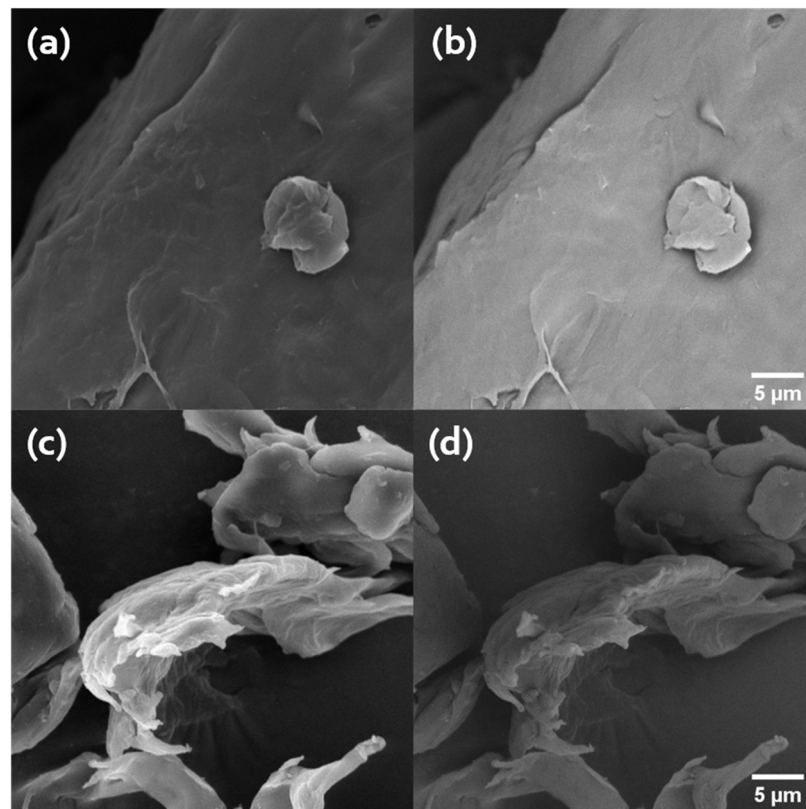
Figure 7. SEM micrographs of LDPE samples—untreated sample scanned in (**a**) SE and (**b**) BSE mode, and photo-Fenton-treated sample scanned in (**c**) SE and (**d**) BSE mode.

The decrease in the intensity of the bands of C–Cl stretching (834 cm^{-1} [74,75]), CH wagging (1427 cm^{-1} [75]), and CH$_2$ wagging (964 cm^{-1} [75]) in the case of treated PVC supports our assumption that dehydrogenation or dehydrochlorination are the initial steps of PVC degradation. Moreover, this corresponds to the formation of the C=C peak at 1620 cm^{-1}, since dehydrochlorination leads to the formation of polyene structures [68,76]. The comparison of the intensities of the monitored band for the PVC treatments shows the higher efficiency of the photo-Fenton treatment compared to the classical Fenton treatment; the apparent reason for this is the introduction of UV-C radiation into the treatment. PVC is considered to be more sensitive to photo-treatment compared to the other two polymers investigated, especially in the wavelength range of 253–310 nm [68], where the irradiation used in this study is located.

In the SEM analysis, we imaged the MPs samples in SE and BSE mode (Figures 7 and 8). Most of the morphologically and texturally relevant changes on the surface of the polymer samples could be evidenced with the SE detector, while compositionally (chemically) relevant changes could be observed with the BSE detector. Drastic changes in the chemical composition were unlikely, but BSE images could indicate relevant areas of degradation. Textural changes were expected.

As can be seen in Figure 7a, the untreated LDPE microparticles have a low surface roughness, and no agglomerates or aggregates are present. Figure 7b shows that the phase composition was highly homogeneous. The photo-Fenton treatment of the LDPE sample led to an increase in surface roughness with additional morphological defects (Figure 7c). The BSE image (Figure 7d) potentially depicts a gradient, indicating a change in composition compared to the reference.
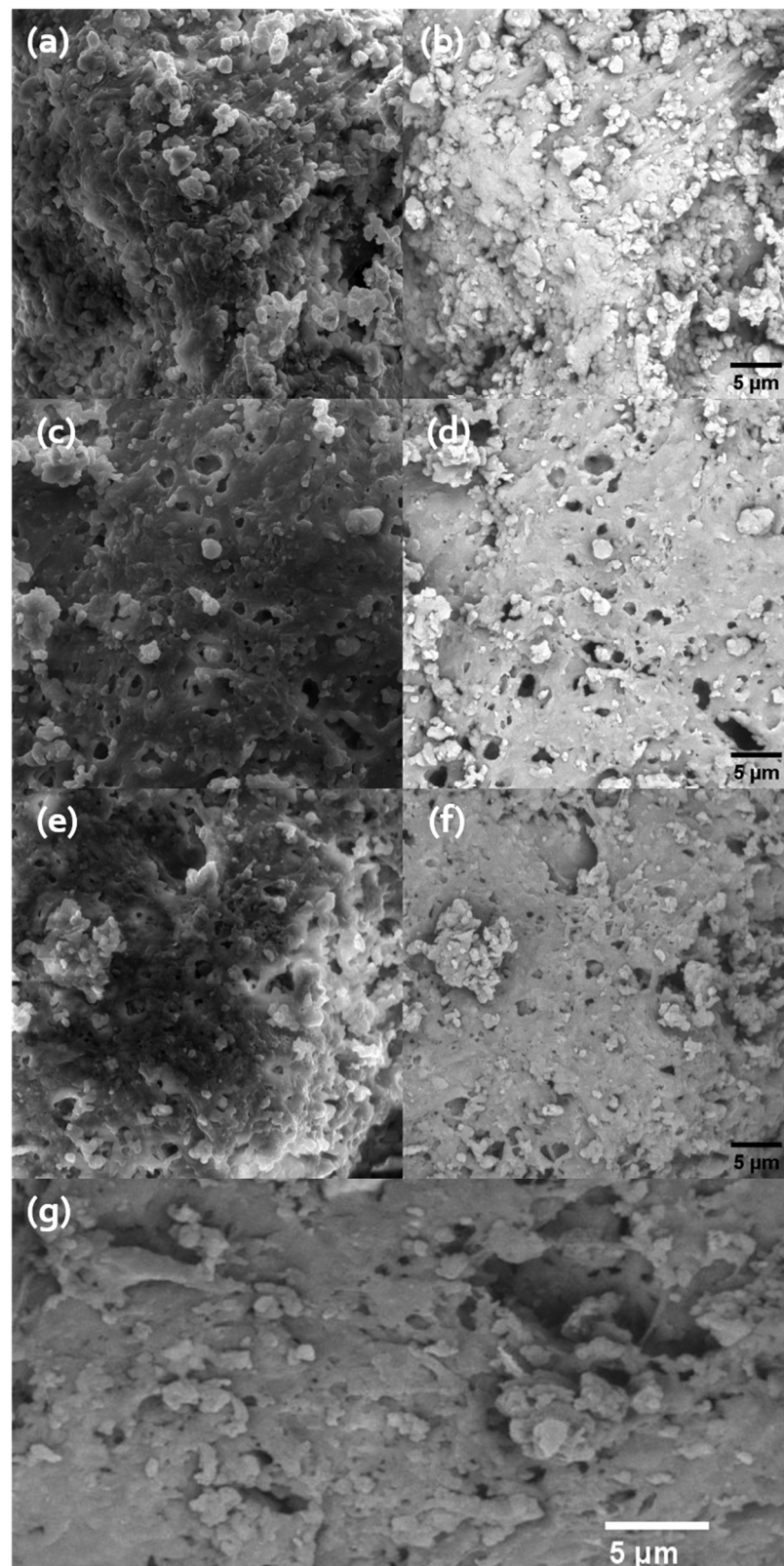
Figure 8. SEM micrographs of PVC samples—untreated sample scanned in (**a**) SE and (**b**) BSE mode, Fenton-treated sample scanned in (**c**) SE and (**d**) BSE mode, and photo-Fenton-treated sample scanned in (**e**) SE and (**f**,**g**) BSE mode.

In contrast to the untreated LDPE MPs, the surface morphology of the untreated PVC MPs scanned in SE mode (Figure 8a) shows considerable roughness and a grainy

morphology, while BSE scanning (Figure 8b) reveals a homogeneous phase composition. Moreover, the influences of the Fenton treatment and the photo-Fenton treatment on the MPs were more evident in the PVC samples. In the case of the Fenton treatment, an increase in surface roughness and apparent porosity can be observed (Figure 8c). The BSE images point to the absence of any compositional phase changes (Figure 8d). In the photo-Fenton treatment (Figure 8e,f), however, the porosity increases even more, together with the surface roughness. The BSE image (Figure 8f) shows possible in-depth compositional phase changes. Figure 8g shows an enlarged view of an area with the most relevant morphological changes observed in Figure 8f. The extended degradation is visible, i.e., the porosity extends beyond the surface of the samples.

5. Conclusions

AOPs are an emerging approach for the remediation of environments polluted by non-biodegradable organic substances [77]. Conventional plastic polymers, especially in the form of micro- and nanoplastics, are non-biodegradable organic pollutants whose presence in the environment has become a global environmental problem [78].

In this study, the potential of Fenton, photo-Fenton, and Fenton-like processes for the degradation of LDPE, PP, and PVC MPs was investigated without going into the analysis of the degradation mechanisms. The treatments lasted 60 min. PP was the least sensitive to the treatments, with no significant changes observed in the intensities of the characteristic FTIR bands. For LDPE, signs of degradation were only observed after the photo-Fenton treatment. The PVC samples were the most sensitive to the treatments, as signs of degradation were observed after the Fenton and photo-Fenton treatments, while the Fenton-like treatment showed no effect. The results indicate that of the three treatments applied, the photo-Fenton treatment is the most efficient in degrading PVC MPs. The SEM analysis of the LDPE samples treated with photo-Fenton and the PVC samples treated with Fenton and photo-Fenton confirmed the changes on the MP surface and even the in-depth changes in the PVC treated with photo-Fenton.

The Fenton-based processes did not prove to be overly efficient in degrading LDPE, PP, and PVC MPs at the selected treatment duration of 60 min. It is likely that extending the treatment would lead to better efficiency, but in this case the question of the economic viability of the treatment arises. Therefore, investigating the potential of some other AOPs, e.g., those combining UV-C radiation with other oxidizing agents, such as ozone, peroxide, or persulfate, seems to be a more promising way to remediate the environment polluted by MPs. However, since this study has shown that the Fenton treatment of PVC and the photo-Fenton treatment of LDPE and PVC have led to some changes in MPs, there is a possibility that these treatments can be efficiently used as pretreatments for biodegradation, as the observed changes could be very beneficial for microbial colonization of the surface of MPs.

Author Contributions: Conceptualization, M.M. (Marinko Markić), Š.U., and D.K.G.; methodology, K.B.M., M.M. (Martina Miloloža), and M.C.; formal analysis, K.B.M., F.R.-P., A.B., and V.M.; writing—original draft preparation, K.B.M.; writing—review and editing, Š.U. and D.K.G.; visualization, K.B.M. and Š.U.; supervision, T.B. and M.U.B.; project administration, T.B. All authors have read and agreed to the published version of the manuscript.

Conflicts of Interest: The authors declare no conflicts of interest.

References

1. Finch, C.E. Evolution of the human lifespan and diseases of aging: Roles of infection, inflammation, and nutrition. *Proc. Natl. Acad. Sci. USA* **2010**, *107*, 1718–1724. [CrossRef]
2. Blagosklonny, M.V. Why human lifespan is rapidly increasing: Solving "longevity riddle" with "revealed-slow-aging" hypothesis. *Aging* **2010**, *2*, 177–182. [CrossRef] [PubMed]
3. United Nations Population Fund, World Population Trends. Available online: https://www.unfpa.org/world-population-trends#readmore-expand (accessed on 20 February 2023).
4. Ukaogo, P.O.; Ewuzie, U.; Onwuka, C.V. Environmental pollution: Causes, effects, and the remedies. In *Microorganisms for Sustainable Environment and Health*; Chowdhary, P., Raj, A., Verma, D., Akhter, Y., Eds.; Elsevier: Chennai, India, 2020; pp. 419–429. [CrossRef]
5. Martinez, J.L. Environmental pollution by antibiotics and by antibiotic resistance determinants. *Environ. Pollut.* **2009**, *157*, 2893–2902. [CrossRef] [PubMed]
6. Chen, J.; Wu, J.; Sherrell, P.C.; Chen, J.; Wang, H.; Zhang, W.-x.; Yang, J. How to Build a Microplastics-Free Environment: Strategiesfor Microplastics Degradation and Plastics Recycling. *Adv. Sci.* **2022**, *9*, 2103764. [CrossRef] [PubMed]
7. Erceg, M.; Tutman, P.; Vojanić Varezić, D.; Bobanović, A. Karakterizacija mikroplastike u sedimentu plaže Prapratno. *Kem. Ind.* **2020**, *69*, 253–260. [CrossRef]
8. Gasperi, J.; Wright, S.L.; Dris, R.; Collard, F.; Mandin, C.; Guerrouache, M.; Langlois, V.; Kelly, F.J.; Tassin, B. Microplastics in air: Are we breathing it in? *Curr. Opin. Environ. Sci. Health* **2018**, *1*, 1–5. [CrossRef]
9. Boots, B.; Russell, C.W.; Green, D.S. Effects of Microplastics in Soil Ecosystems: Above and Below Ground. *Environ. Sci. Technol.* **2019**, *53*, 11496–11506. [CrossRef] [PubMed]
10. Scherer, C.; Weber, A.; Stock, F.; Vurusic, S.; Egerci, H.; Kochleus, C.; Arendt, N.; Foeldi, C.; Dierkes, G.; Wagner, M.; et al. Comparative assessment of microplastics in water and sediment of a large European river. *Sci. Total Environ.* **2020**, *738*, 139866. [CrossRef]
11. Akhbarizadeh, R.; Moore, F.; Keshavarzi, B. Investigating microplastics bioaccumulation and biomagnification in seafood from the Persian Gulf: A threat to human health? *Food Addit. Contam. A* **2019**, *36*, 1696–1708. [CrossRef]
12. Yuan, Z.; Nag, R.; Cummins, E. Human health concerns regarding microplastics in the aquatic environment—From marine to food systems. *Sci. Total Environ.* **2022**, *823*, 153730. [CrossRef]
13. Miller, M.E.; Hamann, M.; Kroon, F.J. Bioaccumulation and biomagnification of microplastics in marine organisms: A review and meta-analysis of current data. *PLoS ONE* **2020**, *15*, e0240792. [CrossRef] [PubMed]
14. Covernton, G.A.; Cox, K.D.; Fleming, W.L.; Buirs, B.M.; Davies, H.L.; Juanes, F.; Dudas, S.E.; Dower, J.F. Large size (>100 μm) microplastics are not biomagnifying in coastal marine food webs of British Columbia, Canada. *Ecol. Appl.* **2022**, *32*, e2654. [CrossRef] [PubMed]
15. Cui, W.; Gao, P.; Zhang, M.; Wang, L.; Sun, H.; Liu, C. Adverse effects of microplastics on earthworms: A critical review. *Sci. Total Environ.* **2022**, *850*, 158041. [CrossRef]
16. Zolotova, N.; Kosyreva, A.; Dzhalilova, D.; Fokichev, N.; Makarova, O. Harmful effects of the microplastic pollution on animal health: A literature review. *PeerJ* **2022**, *10*, e13503. [CrossRef]
17. Lei, L.; Liu, M.; Song, Y.; Lu, S.; Hu, J.; Cao, C.; Xie, B.; Shi, H.; He, D. Polystyrene (nano)microplastics cause size-dependent neurotoxicity, oxidative damage and other adverse effects in *Caenorhabditis elegans*. *Environ. Sci. Nano* **2018**, *5*, 2009–2020. [CrossRef]
18. Rubio-Armendáriz, C.; Alejandro-Vega, S.; Paz-Montelongo, S.; Gutiérrez-Fernández, Á.J.; Carrascosa-Iruzubieta, C.J.; Hardisson-de la Torre, A. Microplastics as Emerging Food Contaminants: A Challenge for Food Safety. *Int. J. Environ. Res. Public Health* **2022**, *19*, 1174. [CrossRef]
19. Bule Možar, K.; Miloloža, M.; Martinjak, V.; Cvetnić, M.; Kušić, H.; Bolanča, T.; Kučić Grgić, D.; Ukić, Š. Potential of Advanced Oxidation as Pretreatment for Microplastics Biodegradation. *Separations* **2023**, *10*, 132. [CrossRef]
20. Poerio, T.; Piacentini, E.; Mazzei, R. Membrane Processes for Microplastic Removal. *Molecules* **2019**, *24*, 4148. [CrossRef]
21. Lupu, G.-I.; Orbeci, C.; Bobirică, L.; Bobirică, C.; Pascu, L.F. Key Principles of Advanced Oxidation Processes: A Systematic Analysis of Current and Future Perspectives of the Removal of Antibiotics from Wastewater. *Catalysts* **2023**, *13*, 1280. [CrossRef]
22. Volke-Sepúlveda, T.; Saucedo-Castañeda, G.; Gutiérrez-Rojas, M.; Manzur, A.; Favela-Torres, E. Thermally treated low density polyethylene biodegradation by *Penicillium pinophilum* and *Aspergillus niger*. *J. Appl. Polym. Sci.* **2002**, *83*, 305–314. [CrossRef]
23. Esmaeili, A.; Pourbabaee, A.A.; Alikhani, H.A.; Shabani, F.; Esmaeili, E. Biodegradation of low-density polyethylene (LDPE) by mixed culture of Lysinibacillus xylanilyticus and Aspergillus niger in soil. *PLoS ONE* **2013**, *8*, e71720. [CrossRef]
24. Ortiz, D.; Munoz, M.; Nieto-Sandoval, J.; Romera-Castillo, C.; de Pedro, Z.M.; Casas, J.A. Insights into the degradation of microplastics by Fenton oxidation: From surface modification to mineralization. *Chemosphere* **2022**, *309*, 136809. [CrossRef]
25. Lang, M.; Yu, X.; Liu, J.; Xia, T.; Wang, T.; Jia, H.; Guo, X. Fenton aging significantly affects the heavy metal adsorption capacity of polystyrene microplastics. *Sci. Total Environ.* **2020**, *722*, 137762. [CrossRef] [PubMed]
26. Piazza, V.; Uheida, A.; Gambardella, C.; Garaventa, F.; Faimali, M.; Dutta, J. Ecosafety Screening of Photo-Fenton Process for the Degradation of Microplastics in Water. *Front. Mar. Sci.* **2022**, *8*, 791431. [CrossRef]
27. Miao, F.; Liu, Y.; Gao, M.; Yu, X.; Xiao, P.; Wang, M.; Wang, S.; Wang, X. Degradation of polyvinyl chloride microplastics via an electro-Fenton-like system with a TiO_2/graphite cathode. *J. Hazard. Mater.* **2020**, *399*, 123023. [CrossRef] [PubMed]

28. Liu, X.; Sun, P.; Qu, G.; Jing, J.; Zhang, T.; Shi, H.; Zhao, Y. Insight into the characteristics and sorption behaviours of aged polystyrene microplastics through three type of accelerated oxidation processes. *J. Hazard. Mater.* **2021**, *407*, 124836. [CrossRef] [PubMed]

29. Amelia, D.; Karamah, E.F.; Mahardika, M.; Syafri, E.; Rangappa, S.M.; Siengchin, S.; Asrofi, M. Effect of advanced oxidation process for chemical structure changes of polyethylene microplastics. *Mater Today Proc.* **2021**, *52*, 2501–2504. [CrossRef]

30. Wang, Q.; Chen, M.; Min, Y.; Shi, P. Aging of polystyrene microplastics by UV/sodium percarbonate oxidation: Organic release, mechanism, and disinfection by-product formation. *J. Hazard. Mater.* **2024**, *464*, 132934. [CrossRef]

31. de Aragão Belé, T.G.; Neves, T.F.; Cristale, J.; Prediger, P.; Constapel, M.; Dantas, R.F. Oxidation of microplastics by O_3 and O_3/H_2O_2: Surface modification and adsorption capacity. *J. Water Process Eng.* **2021**, *41*, 102072. [CrossRef]

32. Ouyang, Z.; Li, S.; Zhao, M.; Wangmu, Q.; Ding, R.; Xiao, C.; Guo, X. The aging behavior of polyvinyl chloride microplastics promoted by UV-activated persulfate process. *J. Hazard. Mater.* **2022**, *424*, 127461. [CrossRef]

33. Kang, J.; Zhou, L.; Duan, X.; Sun, H.; Ao, Z.; Wang, S. Degradation of cosmetic microplastics via functionalized carbon nanosprings. *Matter* **2019**, *1*, 745–758. [CrossRef]

34. Luo, H.; Zeng, Y.; Zhao, Y.; Xiang, Y.; Li, Y.; Pan, X. Effects of advanced oxidation processes on leachates and properties of microplastics. *J. Hazard. Mater.* **2021**, *413*, 125342. [CrossRef] [PubMed]

35. Zhou, L.; Wang, T.; Qu, G.; Jia, H.; Zhu, L. Probing the aging processes and mechanisms of microplastic under simulated multiple actions generated by discharge plasma. *J. Hazard. Mater.* **2020**, *398*, 122956. [CrossRef] [PubMed]

36. Kastanek, F.; Spacilova, M.; Krystynik, P.; Dlaskova, M.; Solcova, O. Fenton Reaction–Unique but Still Mysterious. *Processes* **2023**, *11*, 432. [CrossRef]

37. Deng, Y.; Zhao, R. Advanced oxidation processes (AOPs) in wastewater treatment. *Curr. Pollut. Rep.* **2015**, *1*, 167–176. [CrossRef]

38. Hamd, W.; Daher, E.A.; Tofa, T.S.; Dutta, J. Recent Advances in Photocatalytic Removal of Microplastics: Mechanisms, Kinetic Degradation, and Reactor Design. *Front. Mar. Sci.* **2022**, *9*, 885614. [CrossRef]

39. Mohammed Bello, M.; Abdul Raman, A.A.; Asghar, A. A review on approaches for addressing the limitations of Fenton oxidation for recalcitrant wastewater treatment. *Process Saf. Environ. Prot.* **2019**, *126*, 119–140. [CrossRef]

40. Armstrong, D.A.; Huie, R.E.; Koppenol, W.H.; Lymar, S.V.; Merényi, G.; Neta, P.; Ruscic, B.; Stanbury, D.M.; Steenken, S.; Wardman, P. Standard electrode potentials involving radicals in aqueous solution: Inorganic radicals (IUPAC Technical Report). *Pure Appl. Chem.* **2015**, *87*, 1139–1150. [CrossRef]

41. Kovacic, M.; Kusic, H.; Loncaric Bozic, A.; Dionysiou, D.D. Advanced Oxidation Processes. In *Encyclopedia of Water: Science, Technology, and Society*; Maurice, P.A., Ed.; Wiley: Hoboken, NJ, USA, 2019; Volume 4, pp. 1925–1940. [CrossRef]

42. Garcia-Costa, A.L.; Casas, J.A. Intensification strategies for thermal H_2O_2-based advanced oxidation processes: Current trends and future perspectives. *Chem. Eng. J. Adv.* **2022**, *9*, 100228. [CrossRef]

43. Xu, M.; Wu, C.; Zhou, Y. Advancements in the Fenton Process for Wastewater Treatment. In *Advanced Oxidation Processes—Applications, Trends, and Prospects*; Bustillo-Lecompte, C., Ed.; IntechOpen: Rijeka, Croatia, 2020; pp. 1–17. [CrossRef]

44. Patel, D.; Wu, J.; Chan, P.; Upreti, S.; Turcotte, G.; Ye, T. Surface modification of low density polyethylene films by homogeneous catalytic ozonation. *Chem. Eng. Res. Des.* **2012**, *90*, 1800–1806. [CrossRef]

45. Ameta, R.; Chohadia, A.K.; Jain, A.; Punjabi, P.B. Fenton and Photo-Fenton Processes. In *Advanced Oxidation Processes for Waste Water Treatment: Emerging Green Chemical Technology*; Ameta, S.C., Ameta, R., Eds.; Academic Press: Chennai, India, 2018; pp. 49–87. [CrossRef]

46. Wang, N.; Zheng, T.; Zhang, G.; Wang, P. A review on Fenton-like processes for organic wastewater treatment. *J. Environ. Chem. Eng.* **2016**, *4*, 762–787. [CrossRef]

47. Ribas Fargas, D. In Situ Groundwater Remediation Treatments: Natural Denitrification Study and Nano Zero Valent Iron Production. Ph.D. Thesis, Universitat Politècnica de Catalunya, Barcelona, Spain, 2017.

48. Jang, M.-H.; Lim, M.; Hwang, Y.S. Potential environmental implications of nanoscale zero-valent iron particles for environmental remediation. *Environ. Health Toxicol.* **2014**, *29*, e2014022. [CrossRef]

49. Gacitua, M.; Pavez, L.; Escudey, M.; Antilén, M. Adsorption of Zerovalent Iron Nanoparticles in the Inorganic Fraction of Volcanic Soils. *J. Soil Sci. Plant. Nutr.* **2022**, *22*, 2392–2405. [CrossRef]

50. Kušić, H.; Lončarić Božić, A.; Koprivanac, N. Fenton type processes for minimization of organic content in coloured wastewaters: Part I: Processes optimization. *Dyes Pigment.* **2007**, *74*, 380–387. [CrossRef]

51. Fentons Reagent General Chemistry Using H_2O_2. Available online: https://www.h2o2.com/pages.aspx?pid=143&name=General-Chemistry-of-Fenton-s-Reagent (accessed on 7 July 2023).

52. Eyjolfsson, R. Chapter One—Introduction. In *Design and Manufacture of Pharmaceutical Tablets*; Eyjolfsson, R., Ed.; Academic Press: London, UK, 2015; pp. 1–28. [CrossRef]

53. Miloloža, M.; Ukić, Š.; Cvetnić, M.; Bolanča, T.; Kučić Grgić, D. Optimization of Polystyrene Biodegradation by *Bacillus cereus* and *Pseudomonas alcaligenes* Using Full Factorial Design. *Polymers* **2022**, *14*, 4299. [CrossRef]

54. Bule Možar, K.; Miloloža, M.; Martinjak, V.; Cvetnić, M.; Ocelić Bulatović, V.; Mandić, V.; Bafti, A.; Ukić, Š.; Kučić Grgić, D.; Bolanča, T. Bacteria and Yeasts Isolated from the Environment in Biodegradation of PS and PVC Microplastics: Screening and Treatment Optimization. *Environments* **2023**, *10*, 207. [CrossRef]

55. Cvetnic, M.; Ukic, S.; Kusic, H.; Bolanca, T.; Loncaric Bozic, A. Photooxidative Degradation of Pesticides in Water; Response Surface Modeling Approach. *J. Adv. Oxid. Technol.* **2017**, *20*, 20160172. [CrossRef]

56. Markic, M.; Cvetnic, M.; Ukic, S.; Kusic, H.; Bolanca, T.; Loncaric Bozic, A. Influence of process parameters on the effectiveness of photooxidative treatment of pharmaceuticals. *J. Environ. Sci. Health A* **2018**, *53*, 338–351. [CrossRef] [PubMed]

57. Miloloža, M.; Bule, K.; Ukić, Š.; Cvetnić, M.; Bolanča, T.; Kušić, H.; Ocelić Bulatović, V.; Kučić Grgić, D. Ecotoxicological Determination of Microplastic Toxicity on Algae *Chlorella* sp.: Response Surface Modeling Approach. *Water Air Soil Pollut.* **2021**, *232*, 327. [CrossRef]

58. Liu, X. *Organic Chemistry I*; Kwantlen Polytechnic University: Surrey, BC, Canada, 2021; p. 198.

59. Celina, M.C.; Linde, E.; Martinez, E. Carbonyl Identification and Quantification Uncertainties for Oxidative Polymer Degradation. *Polym. Degrad. Stab.* **2021**, *188*, 109550. [CrossRef]

60. Kumari, A.; Chaudhary, D.R.; Jha, B. Destabilization of polyethylene and polyvinylchloride structure by marine bacterial strain. *Environ. Sci. Pollut. Res.* **2019**, *26*, 1507–1516. [CrossRef]

61. Subramani, M.; Sepperumal, U. FTIR analysis of bacterial mediated chemical changes in Polystyrene foam. *Ann. Biol. Res.* **2016**, *7*, 55–61.

62. Lu, J.; Ma, S.; Gao, J. Study on the Pressurized Hydrolysis Dechlorination of PVC. *Energy Fuels* **2002**, *16*, 1251–1255. [CrossRef]

63. Dobberphul, H. *Organic Chemistry—MLC*; Martin Luther College: New Ulm, MN, USA; p. 3.1.12.1. Available online: https://chem.libretexts.org/Courses/Martin_Luther_College/Organic_Chemistry_-_MLC/03:_Alcohols_Ethers_Thiols_Sulfides_and_Amines/3.01:_Alcohols_and_Phenols/3.1.12:_Spectroscopy_of_Alcohols_and_Phenols (accessed on 16 February 2024).

64. Gaumet, S.; Gardette, J.-L. Photo-oxidation of poly(vinyl chloride): Part 2—A comparative study of the carbonylated products in photo-chemical and thermal oxidations. *Polym. Degrad. Stab.* **1991**, *33*, 17–34. [CrossRef]

65. Ahmed, A.; El-Hiti, G.A.; Hadi, A.G.; Ahmed, D.S.; Baashen, M.A.; Hashim, H.; Yousif, E. Photostabilization of Poly(vinyl chloride) Films Blended with Organotin Complexes of Mefenamic Acid for Outdoor Applications. *Appl. Sci.* **2021**, *11*, 2853. [CrossRef]

66. Zhang, Y.; Pedersen, J.N.; Eser, B.E.; Guo, Z. Biodegradation of polyethylene and polystyrene: From microbial deterioration to enzyme discovery. *Biotechnol. Adv.* **2022**, *60*, 107991. [CrossRef]

67. Ainali, N.M.; Bikiaris, D.N.; Lambropoulou, D.A. Aging effects on low- and high-density polyethylene, polypropylene and polystyrene under UV irradiation: An insight into decomposition mechanism by Py-GC/MS for microplastic analysis. *J. Anal. Appl. Pyrolysis* **2021**, *158*, 105207. [CrossRef]

68. Yousif, E.; Hasan, A. Photostabilization of poly(vinyl chloride)—Still on the run. *J. Taibah Univ. Sci.* **2015**, *9*, 421–448. [CrossRef]

69. Payne, L.B. The Dehydrochlorination Mechanism of the Internal Allylic Chloride Structure in Poly(vinyl chloride). Ph.D. Thesis, College of William & Mary, Williamsburg, VA, USA, 2020. [CrossRef]

70. Li, X.; Wang, J.; Rykov, A.I.; Sharma, V.K.; Wei, H.; Jin, C.; Liu, X.; Li, M.; Yu, S.; Sun, C.; et al. Prussian blue/TiO_2 nanocomposites as a heterogeneous photo-Fenton catalyst for degradation of organic pollutants in water. *Catal. Sci. Technol.* **2015**, *5*, 504–514. [CrossRef]

71. Kowalska, B.; Klepka, T.; Kowalski, D. Influence of chlorinated water on mechanical properties of polyethylene and polyvinyl chloride pipes. *WIT Trans. Built Environ.* **2016**, *165*, 63–74. [CrossRef]

72. Jia, X.; Qin, C.; Friedberger, T.; Guan, Z.; Huang, Z. Efficient and selective degradation of polyethylenes into liquid fuels and waxes under mild conditions. *Sci. Adv.* **2016**, *2*, e1501591. [CrossRef]

73. Burelo, M.; Hernández-Varela, J.D.; Medina, D.I.; Treviño-Quintanilla, C.D. Recent developments in bio-based polyethylene: Degradation studies, waste management and recycling. *Heliyon* **2023**, *9*, e21374. [CrossRef]

74. Ul-Hamid, A.; Soufi, K.Y.; Al-Hadhrami, L.M.; Shemsi, A.M. Failure investigation of an underground low voltage XLPE insulated cable. *Anti-Corros. Method. M.* **2015**, *62*, 281–287. [CrossRef]

75. Li, T.; Zhao, P.; Lei, M.; Li, Z. Understanding Hydrothermal Dechlorination of PVC by Focusing on the Operating Conditions and Hydrochar Characteristics. *Appl. Sci.* **2017**, *7*, 256. [CrossRef]

76. Yaseen, A.A.; Yousif, E.; Al-Tikrity, E.T.B.; El-Hiti, G.A.; Kariuki, B.M.; Ahmed, D.S.; Bufaroosha, M. FTIR, Weight, and Surface Morphology of Poly(vinyl chloride) Doped with Tin Complexes Containing Aromatic and Heterocyclic Moieties. *Polymers* **2021**, *13*, 3264. [CrossRef]

77. Kumari, P.; Kumar, A. ADVANCED OXIDATION PROCESS: A remediation technique for organic and non-biodegradable pollutant. *Results Surf. Interfaces* **2023**, *11*, 100122. [CrossRef]

78. Ma, Y.-B.; Xie, Z.-Y.; Hamid, N.; Tang, Q.-P.; Deng, J.-Y.; Luo, L.; Pei, D.-S. Recent advances in micro (nano) plastics in the environment: Distribution, health risks, challenges and future prospects. *Aquat. Toxicol.* **2023**, *261*, 106597. [CrossRef] [PubMed]